Kinetics of the 3C-6H polytypic transition in 3C-SiC single crystals: a diuse X-ray scattering study

D. Dompoint, Alexandre Boulle, I. Galben-Sandulache, D. Chaussende, L. T M Hoa, T. Ouisse, D. Eyidi, J.L. Demenet, M.F. Beaufort, J. Rabier

Kinetics of the 3C-6H polytypic transition in 3C-SiC single crystals: a diffuse X-ray scattering study

D. Dompoint,[1] A. Boulle,[1, a)] I. Galben-Sandulache,[2] D. Chaussende,[2] L. T. M. Hoa,[2] T. Ouisse,[2] D. Eyidi,[3] J. L. Demenet,[3] M. F. Beaufort,[3] and J. Rabier[3]

[1)] *Science des Procédés Céramiques et de Traitements de Surface (SPCTS)*
CNRS UMR 6638, Centre Européen de la Céramique
12,rue Atlantis 87068 LIMOGES,France

[2)] *Laboratoire des Matériaux et du Génie Physique (LMGP)*
CNRS UMR 5628, Grenoble INP, Minatec,
3 parvis Louis Néel, BP 257, 38016 Grenoble Cedex 01,
France

[3)] *Institut Pprime*
CNRS UPR 3346, Université de Poitiers, Département Physique et Mécanique des Matériaux
SP2MI-Téléport 2-Bd Marie et Pierre Curie, BP 30179,
86962 Futuroscope-Chasseneuil Cedex,France

(Dated: July 22, 2011)

In this work, the kinetics of the 3C-6H polytypic transition in 3C-SiC single crystals are studied in details by means of diffuse X-ray scattering (DXS) coupled with numerical simulations and transmission electron microscopy and optical birefringence microscopy. Upon high-temperature annealing, spatially correlated stacking faults (SFs), lying in the {111} planes, are generated within the crystal and tend to form bands of partially transformed SiC. It is shown that the numerical simulation of the DXS curves allows to unambiguously deduce the transformation level within these bands, as well as the volume fraction corresponding to these bands. Increasing annealing time results (i) in the growth of the partially transformed regions by the glide of the partials dislocations bounding the SFs, and (ii) in the generation of new SFs within the crystal by means of a double-cross slip motion. The kinetics of each of these mechanisms are presented and discussed with respect to the annealing temperature, the initial SF density and crystalline quality.

[a)] alexandre.boulle@unilim.fr

I. INTRODUCTION

The cubic polytype of silicon carbide (3C-SiC) exhibits attractive chemical, thermal and electrical properties which make it an ideal candidate for high-power and high-frequency operating devices, such as metal-oxide semiconductor field-effect transistors (MOSFETs)[1]. In the recent years important efforts have therefore been directed to characterizing the electronic[2,3] and structural properties of 3C-SiC[4–6] and as well as their mutual interactions[7–10]. However, despite this undeniable interest and several decades of studies, the growth of high-quality 3C-SiC single crystals still remains an extremely challenging task. It is now commonly admitted that this difficulty stems from the high temperatures (>1900°C) that are required to grow SiC single crystals from the vapor phase, where the 3C polytype is known to be unstable[11]. These high temperatures trigger the 3C-6H polytypic transition, which takes place by the formation and extension of stacking faults (SFs), resulting in crystals of poor structural quality. The presence of SFs are in turn known to have deleterious effects on the performances of 3C-SiC-based MOSFETs[7] which obviously limits the appeal of 3C-SiC for actual devices. A detailed understanding of the 3C-6H transition, both in terms of the mechanisms involved and transformation kinetics, is hence a key issue for the development of high-quality 3C-SiC materials.

The 3C-6H polytypic transition has been thoroughly studied in the case of polycrystalline materials[11] mainly using transmission electron microscopy (TEM) and powder diffraction. It has been demonstrated that in such materials the transitions take place by surface or vapor-phase diffusion with activation energies lying in the 495 - 661 kJ/mol (5.13 - 6.85 eV) range[11]. On the contrary, studies dealing with the transformation of 3C-SiC single crystals are extremely scarce and, to the best of our knowledge, the question of the transformation kinetics has not been addressed to date. This lack of experimental data regarding the 3C-6H polytypic transition in single crystals is due (i) to the above-mentioned difficulties to grow 3C-SiC single crystals and (ii) to the lack of quantitative characterization tools that would allow to obtain quantitative information concerning the transformation (transformation level and polytype volume fraction). Qualitative information, for instance regarding the transformation mechanism or the nature of the polytypes that are formed, have been obtained using TEM[12], Raman scattering[13,14] or X-ray rotation photography[15]. Besides, these studies reached contradictory conclusions concerning the transformation mechanism.

In a previous study we demonstrated the potential of diffuse X-ray scattering (DXS) for the study of the 3C-6H polytypic transition[16]. DXS, combined with numerical simulations, allows not only to unambiguously determine the transformation mechanism, but also to obtain the transformation level and the polytype volume fraction.

The purpose of the present article is to provide a detailed analysis of the 3C-6H polytypic transition using DXS, supported by TEM and optical birefringence microscopy. A particular emphasis is laid on the transformation kinetics and the mechanisms involved. Experimental details regarding the 3C-SiC single crystals, the thermal treatments and structural characterizations (DXS, TEM and birefringence microscopy) are given in section 2. In section 3, the simulation methodology is briefly recalled and the 3C-6H transition is studied in details. In particular, we shall show that this transition is driven by the nucleation and expansion of partial dislocations bounding stacking faults (SFs). Whereas the expansion of existing SFs dominates in the 'low temperature' regime ($<$2000°C), in the 'high temperature' regime ($>$2000°C) the transformation is mainly driven the nucleation of new SFs. The influence of temperature and crystalline quality will be discussed.

II. EXPERIMENTAL DETAILS

A. 3C-SiC single crystals

In this work we used 10×10 mm^2, 250 μm – thick, commercially available (001)-oriented 3C-SiC single crystals (HAST Corporation) grown by chemical vapor deposition on "undulant" (001) Si wafers (which are removed by polishing subsequently to deposition)[1,17]. The undulant (001) Si substrates exhibit trenches running parallel to the [1-10] direction which allows to significantly reduce the density of the defects which are usually encountered in the heteroepitaxial growth of 3C-SiC on (001) Si, namely anti-phase boundaries (APBs) and SFs lying in the { 111 } planes. It must however be mentioned that this growth process produces highly anisotropic single crystals. Firstly, because defect annihilation takes place progressively during growth, the region close to the SiC/Si interface (hereinafter designated as the 'lower side') exhibits a high density of APBs, SFs and twin boundaries[18], whereas the region close to the SiC surface (hereinafter designated as the 'upper side') exhibits a far better crystalline quality[19]. Secondly, the trenches being parallel to the [1-10] direction, the

annihilation mechanism is only efficient for those SFs lying in the (111) and (-1-11) planes, whereas those lying in the (-111) and (1-11) planes are not affected. Consequently on the upper side of the crystals the SF density is higher along the [1-10] direction (6.4×10^3 cm^{-1}) than along the [110] direction (1.4×10^3 cm^{-1})[20]. The influence of this anisotropic crystalline quality (i.e. upper side vs. lower side and [110] vs. [1-10]) on the polytypic transition will be discussed in the next section.

Two sets of samples (coming from two distinct wafers) have been studied in this work. The first set (from wafer 1) is composed of a raw crystal and 4 crystals annealed at 2000°C for 1, 2, 4 and 8 hour(s) respectively, so as to promote the 3C-6H transition and monitor the transformation kinetics. The second set of samples (from wafer 2) is composed of 4 crystals annealed 5 hours at 1700, 1800, 1900 and 2100°C, respectively. This second set of crystals allows to investigate the thermal behavior of the transition (because of the limited number of 3C-SiC single crystals, it was not possible to record the full transformation kinetic for each temperature). The annealing experiments were conducted under 60 kPa of Argon. The surface of the sample is slightly graphitized upon annealing. The graphite layer is removed before subsequent characterizations.

The uncertainties on the derived transformation levels have been roughly estimated from the fluctuations observed in the raw (non-annealed) crystals originating from the same wafers. Is is important to notice that significant differences are observed when considering crystals from different wafers (up to 20% in the polytype volume fraction in the worst cases). In particular the crystalline quality of wafer 2 turned out to be significantly worse than for wafer 1 (with a SF density reaching 3×10^5 cm^{-1}), so that the results of both set of crystals can not be quantitatively compared. For crystals from the same wafer, the fluctuations can be as high as 10% for the polytype volume fraction.

B. Structural characterizations

DXS experiments have been conducted on a home-made high-resolution diffractometer mounted on a high power x-ray source coupled with a four reflections Ge (220) monochromator and equipped with a curved position sensitive detector (PSD)[21,22]. The x-ray beam is 100 μm thick and 10 mm wide. This diffractometer allows to record wide-range reciprocal space maps (RSMs) including the (002) and (113) reflections of 3C-SiC in a small amount

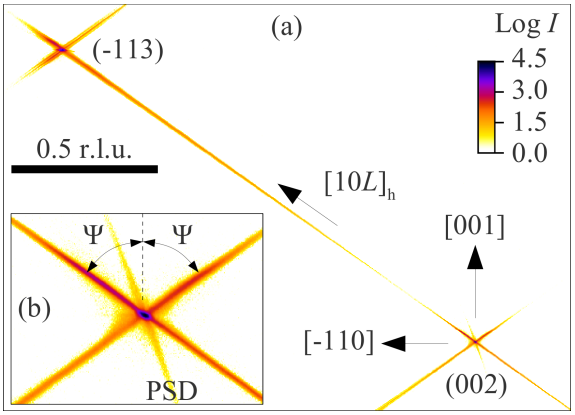

Figure 1. (a) reciprocal space map of a 3C-SiC single crystal annealed 5h at 1900°C. The diffuse streak joining the (002) and (-113) reflections is clearly visible. (b) zoom on the (002) reflections. Two equivalent streaks, making an angle $\psi = 54.74°$ with the [001] direction are due to SFs lying in the (-111) and (1-11) planes. The streak labeled 'PSD' is due to the transmittance function of the detector. Apart from the Bragg reflections and the DXS originating from the SFs, no other signal is detected.

of time[23]. A typical reciprocal space map of a partially transformed 3C-SiC single crystal is displayed in Fig. 1.

In the following we shall make use of the usual hexagonal unit-cell, the c-axis of which is parallel to the [111] direction of the cubic unit-cell and corresponds to the stacking direction of the Si-C bilayers[12] (the relations between the standard cubic and hexagonal unit cells are given in Ref.[24]). Within this unit cell, the row joining the (002) and the (113) reflections actually corresponds to the $[10L]_h$ direction (the subscript 'h' stands for hexagonal) where the Bragg reflections occur at $L = 2$ and $L = 5$, respectively (Fig. 1). This direction contains all information regarding the stacking sequence of close-packed structures and is commonly used to monitor polytypic transitions[25]. The intensity distribution along the $[10L]_h$ direction is extracted from the RSM for each sample and for each orientation of the sample (i.e. with either the [110] or the [1-10] parallel to the incident beam and with either the upper or the lower side exposed to the incident beam). These $[10L]_h$ - scans are then simulated with a numerical model in order to extract the polytype volume fraction and the level of transformation. The penetration depth of the X-ray beam varies from 12 μm to 24 μm when moving from the (113) to the (002) reflection. This ensures that the data recorded

from the upper or the lower side are indeed representative of these regions (i.e. we do not integrate over whole thickness of the crystals).

Thin specimen have been prepared for birefringence microscopy observation in a transmission geometry. As the cubic lattice of perfect 3C-SiC is not birefringent, this method is particularly adapted to evidence any increase in the hexagonality of the structure[26]. Two different 50μm thick samples have been cut and mechanically polished from an as-received substrate: one cross section parallel to the original trenches (i.e. parallel to [1-10]) and one planar view (from the upper face). Highly birefringent lamellae can be observed and correspond to regions with non-zero hexagonality (i.e. partially transformed 3C), Figure 2. It can be seen that those lamellae emerge to the upper face but do not propagate down to the lower face.

Transmission Electron Microscopy (TEM) experiments were carried out on a 3C-SiC sample annealed at 1800°C. It was prepared in <001> plane-view as well as in cross-section with <110> as foil normal. The cross-sectional sample was prepared as follows: three pieces of $0.65\times1.0\times2.5$ mm^3 in size were cut and glued together, then mechanically thinned down to 20 μm, prior to argon ion-milling to electron transparency. TEM observations were performed in bright-field and weak-beam dark-field modes on a JEOL 2200-FS TEM equipped with a field-emission gun (FEG), an in-column Omega filter and a Scanning Transmission Electron Microscopy (STEM) unit. All images and diffraction patterns were elastically filtered with a 10 eV slit around the zero-loss peak.

III. RESULTS AND DISCUSSION

A. Diffuse X-ray scattering

The 3C-6H transition occurs through the generation and extension of SFs and, in order to produce the final 6H phase, the SFs have to be spatially correlated. The existence of spatial correlations between SFs gives rise to extended diffuse scattering in the $[10L]_h$ direction. The analysis of this diffuse scattering allows in principle to recover the statistical properties of the stacking sequence and hence to deduce the exact nature of the mechanism responsible for the generation and extension of SFs, as well as the progress of the transition. In a previous study[16] we have demonstrated that the SFs are produced by the glide of partial

dislocations. In this section we briefly recall the physical basis of the model used in this work to simulate the DXS curves and show how it allows to obtain the transformation level of SiC single crystals. The intensity distribution along the $[10L]_h$ row can be written[24]:

$$I(L) = k.PV \int dL'.R(L')I_s(L - L') + b \tag{1}$$

where the scale factor k , and the background b are constant for a given set of experimental conditions. P is the polarization and V the irradiated volume. $I_s(L)$ is the intensity scattered from the sample which is convoluted with the resolution of the diffractometer $R(L)$. The resolution of diffractometer has been described in details elsewhere[22]. In the present case it is very well described by a Gaussian function with FWHM (full width at half maximum) = 0.006 close to the L=2 peak and FWHM=0.01 close to the L=5 peak. An optical micrograph of a partially transformed 3C single crystals is shown in Figure 2. This figure clearly reveals that the transformation does not affect the whole crystal, but instead there are bands of transformed SiC which coexist with regions of pure 3C-SiC. We will show in the following that the polytype contained in these transformed regions do not correspond to pure 6H but rather to partially transformed, i.e. disordered, 3C-SiC. These bands are inclined by $\sim 55°$ with respect to surface, which corresponds to the angle between the (111) and (001) crystallographic planes (54.74°). The scattering from such crystals can hence be described as the superposition of the coherent scattering I_c emanating from the untransformed regions, and the diffuse scattering I_d originating from the transformed regions:

$$I_s(L) = x_t I_d(L) + (1 - x_t)I_c(L) \tag{2}$$

where x_t is the volume fraction of transformed SiC.

In the case of a dislocation-based transformation mechanism, the diffuse intensity can be written as:

$$I_d(L) = 2\psi^2 \Re \left\{ \frac{1}{2} + \frac{\sum_{n=1}^{5} \sum_{m=0}^{n-1} a_{6-n} J_{n-m} exp\left[-2\pi i \left(6 - m\right) L/3\right] - a_0 J_0}{\sum_{n=0}^{6} a_n exp\left[-2\pi i n L/3\right]} \right\} \tag{3}$$

ψ^2 is proportional to the structure factor of a single Si-C bilayer. The coefficients a and J are function of the transformation level τ ($\tau = 0$ for the 3C phase, $\tau = 1$ for the 6H phase) as follows: $a_0 = -\tau^2, a_1 = -\omega\tau(1 - \tau), a_2 = a_3 = a_4 = 0, a_5 = -\omega(1 - \tau), a_6 = 1$

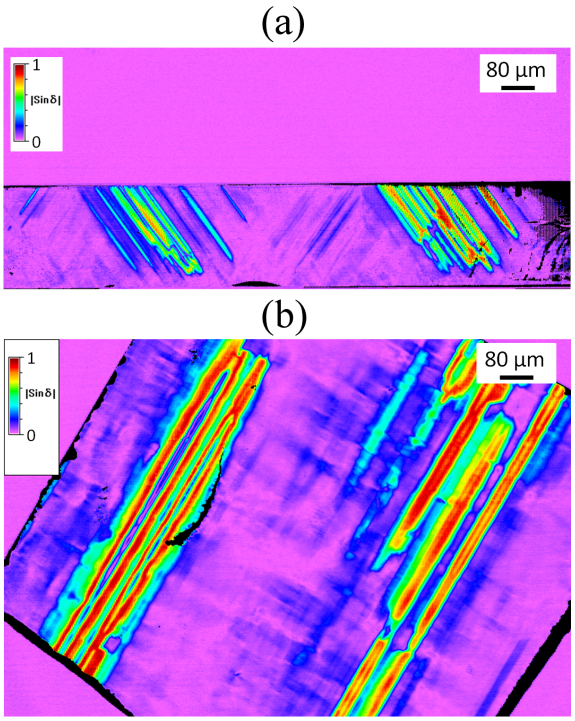

Figure 2. Optical birefringence micrograph of a partially transformed 3C-SiC single crystal. (a) cross-sectional view, (b) plane view. δ is the magnitude of birefingence ($\delta = 0$ corresponds to cubic regions, and $\delta > 0$ corresponds to regions with non-zero hexagonality, i.e. partially transformed regions)

and $J_0 = 1, J_1 = (-2\tau + \tau^2\omega^2 + \omega)/D, J_2 = (\tau + \omega^2 + \tau^2\omega)/D, J_3 = (1-\tau)^2/D, J_4 = (1-\tau)(\omega - 2\tau\omega + \tau)/D, J_5 = \{(1-\tau)[\omega^2(1-3\tau) + 2\tau(\omega - \tau)] - \tau^2(1+2\tau)\}/D$, where $\omega = exp(2\pi i/3)$ and $D = (1+\tau)^2 + 2\tau$. Equation (3) is related to the difference-equation approach of faulting in fcc and hcp metals as described by Warren[24]. Its derivation is based on the treatment introduced by Holloway[27] which does not require an explicit solution for the difference-equation and allows to express the diffracted intensity as a function of the coefficients of the difference-equation and the coefficients of the pair-correlation function (a and J, respectively). Further details can be found in ref[15] and ref[23]. Finally, the coherent scattering I_c can be straightforwardly calculated assuming particular mosaic domain shape and size[28]. In the present case, cubic parallelepipeds with an edge length ranging between 500 nm and 6 μm (depending on the sample and on the transformation level) were found to give excellent agreement with experimental data.

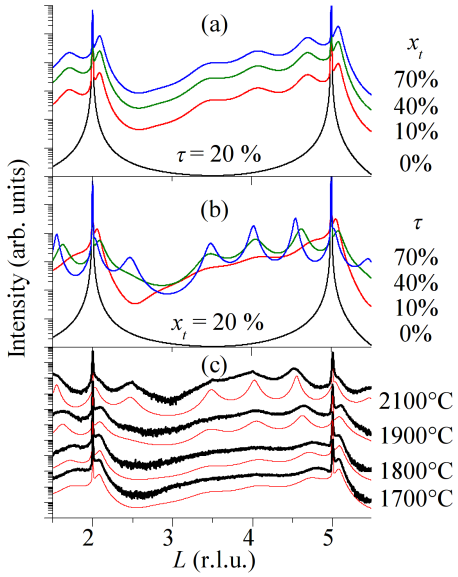

Figure 3. Influence of the polytype volume fraction x_t (a) and the transformation level τ (b) on the DXS profiles. For these calculations τ (respectively x_t) is kept constant and equal to 20% while x_t (respectively τ) successively takes the following values: 0, 10, 40 and 70 %. The curves are normalized to the same maximum value. Increasing x_t results in a simple increase of the diffuse intensity, whereas increasing τ results in a structuring of the diffuse intensity.(c) Experimental (black thick line) and simulated (thin red line) intensity distribution along the $[10L]_h$ row corresponding to samples annealed at 1700, 1800, 1900 and 2100°C, respectively. The curves are shifted vertically for clarity.

As can be anticipated from figure 2, the 3C-6H transition may operate in two ways: either by increasing the transformation level within the partially transformed regions (increasing τ), or by a growth of the transformed regions at the expense of the pure 3C regions (increasing x_t). The global transformation level is given by τx_t. Obviously, for the transition to reach completion, both mechanisms have to take place simultaneously.

Simulations using the previous equations are shown in Figure 3. DXS curves are calculated for increasing polytype volume fraction (a) and increasing transformation level (b). In the case where either x_t or τ is equal to 0, only coherent scattering is present with the Bragg peaks occurring at $L = 2$ and $L = 5$. On the contrary, as soon as τx_t is non zero then diffuse scattering (located between the Bragg peaks) appears. The remaining narrow

Bragg peaks are due to the untransformed parts of the crystals. For a fixed transformation level (20%) the growth of the transformed regions simply results in an increase of the diffuse intensity with a concomitant decrease of the coherent intensity (while the shape of the diffuse scattering remains unchanged). Conversely, an increase of the transformation level at a fixed volume fraction (20%) results in a structuring of the diffuse intensity (while the overall diffuse and coherent intensities remains constant). In this latter case, pseudo-peaks corresponding to the Bragg peaks of the forthcoming 6H phase, emerge from the diffuse intensity. These peaks are more pronounced for high values of τ and their location shifts towards their definitive value corresponding to the 6H phase.

Figure 3 (c) depicts the evolution of the DXS curves recorded from the second set of crystals (wafer 2) which have been annealed 5h for increasing temperature. In agreement with the previous simulations, the narrow peaks located at $L = 2$ and $L = 5$ correspond to the Bragg peaks emanating from untransformed parts of the crystal, whereas the intensity located between these peaks correspond to the diffuse scattering coming from the transformed regions of the crystal. Increasing the temperature results in an overall increase of the diffuse intensity (i.e. a growth of the transformed regions) as well as a structuring of the diffuse intensity (i.e. an increase of the transformation level). It can be seen that the simulation fits the data very well which allows to deduce the polytype volume fraction, which increases from 36 to 56%, and the transformation level, which increases from 15 to 70%. It can be noticed that for the higher temperature (2100°C) the simulation underestimates the width of the pseudo-peaks in the high-L region. This discrepancy is very probably due to the heterogeneous strain field associated to the partial dislocations (the effect of strain-induced broadening being more pronounced for high values of L[29]). Indeed for this temperature we have a transformation level $\tau = 70\%$ which corresponds to a very high density of SFs (i.e. 35% of the lattice planes contain a SF) and hence a very high density of dislocations. The peak broadening associated to the strain field of the dislocations can not be straightforwardly included in the simulation which explains this discrepancy. Recent Monte-Carlo simulations allowed to confirm this hypothesis of strain-induced broadening and will be presented in a separate paper. It should be noted that this effect does not affect the determination of x_t and τ since these parameters are principally deduced from the fit in the low-L region[23] where strain-induced broadening is not significant.

B. Transformation kinetics

The DXS curves recorded from the different crystals (and crystal orientations) have been simulated with the model described earlier, and the transformation level τ and the volume fraction x_t have been deduced in each case. The results obtained from the first set of crystals (wafer 1) are depicted in Fig. 4, whereas those obtained from the second set (wafer 2) are depicted in Fig. 5.

Let us first consider the evolution of τ for increasing annealing time, Fig. 4 (a). In all cases considered, the transformation level behaves in a similar fashion: it increases rapidly and reaches a level of 75-90% after 8 hours at 2000°C. The data have been fitted with a power-law, kt^n (where k is the growth rate and n the kinetic exponent, dashed line in Fig. 4). It turned out that n varies from 0.08(1) to 0.11(2) (the number in brackets indicates the uncertainty on the last digit), i.e. the transformation mechanism is almost independent on the initial SF density ([1-10] vs. [110]) and on the crystalline quality (upper side vs. lower side). A very different behavior is obtained for x_t (Fig. 4 (b)). The fastest kinetic is obtained on the upper side in the [1-10] direction (i.e. the direction with a high SF density), where x_t reaches only 33% after 8 hours at 2000°C. Conversely the slowest kinetic has been observed for the [110] direction ($x_t = 2.5\%$ in 8 hours). This can be explained by the fact that in this direction the SF density is very low, the crystal is hence only weakly transformed, even for long annealing times. On the lower side, the volume fraction is also very low ($x_t = 4.7\%$ in 8 hours) though for a completely different reason. The poor quality of the 3C-SiC crystals on their lower side (mosaicity, presence of twin boundaries and anti-phase boundaries) hinders the motion of dislocations, and hence the expansion of SFs. This can be clearly seen from Fig. 2 where the bands of partially transformed SiC fail to reach the lower side of the crystal. A similar observation has been made by Raman scattering on similar crystals[14].

The activation energies for both mechanisms have been obtained from an Arrhenius plot of the data recorded from the second set of crystals (wafer 2) : $ln(x)$ (where x corresponds to either τ or x_t) is plotted vs. $1/T$ (Fig. 5). For the upper side of the crystal, Fig. 5 (a), despite the scatter of the data corresponding to x_t (due the inhomogeneity of the crystals), it turns out that the transformation mechanisms are characterized by significantly different activation energies, i.e. 1.5(1) eV for the transformation level and 0.5(4) eV for the volume fraction. It can already be mentioned that these values are in good agreement

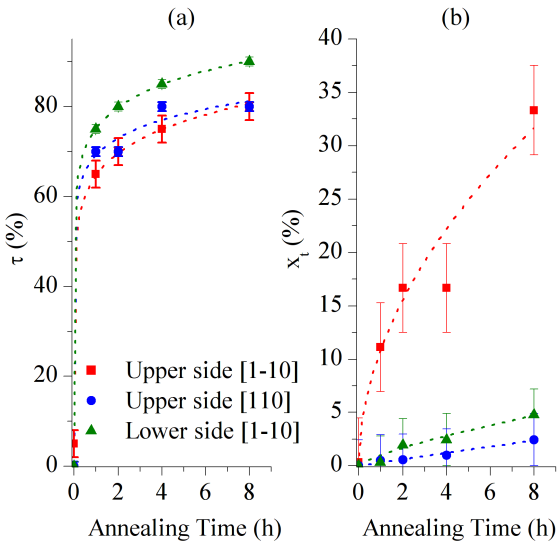

Figure 4. Evolution of the transformation level τ (a) and the the volume fraction x_t (b) as function of annealing time at 2000°C. Squares: upper side, high SF density [1-10]; circles: upper side, low SF density [110]; triangles: lower side. The dotted line is a fit with a power-law.

with the range of values obtained for the activation energy corresponding to the glide of partial dislocation in SiC, either experimentally in hexagonal polytypes[30,31] or in 3C-SiC using numerical simulations[32,33]. This will be discussed in more details in the next section. The interpolation lines cross at $\sim$ 2000°C: for T $>$ 2000°C the transition is driven by the increase of the transformation level within the partially transformed regions τ (characterized by a fast kinetic), whereas for T $<$ 2000°C the transformation is driven by the expansion of the partially transformed regions (increase of x_t, which is characterized by a slow kinetic). As a consequence, high-quality 3C-SiC single crystals may remain kinetically stable when annealed at temperatures lower than 2000°C. This is in good agreement with the observation that high-quality 3C-SiC single crystal are indeed stable upon annealing at 1800°C and 1900°C[23].

On the lower side, Fig. 5 (b), both activation energies are close to each other and significantly higher (2.8(2) eV for τ and 2.4(2) eV for x_t). As above, this can be explained by the fact that on the lower side the dislocations are pinned by structural defects which hinders their motion. An additional energy is therefore required for the dislocations to detach from defects. It is surprising that although the activation energy of τ is increased, the transformation kinetic, Fig. 4 (a), is not affected by the structural quality of the crystal.

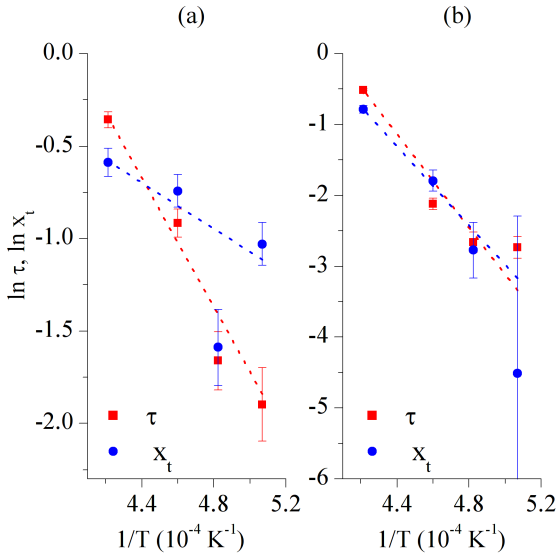

Figure 5. Arrhenius plot of the transformation level τ (squares) and volume fraction x_t (circles) obtained from the upper side (a) and the lower side (b).

The reason for this discrepancy stems from the fact that the data have been obtained from two distinct wafers, with different structural qualities. In particular the activation energies have been obtained from a wafer with a much poorer crystalline quality (with a defect density $\sim$ 100 times higher) where dislocation pinning is very important. It can hence be expected that if the transformation kinetics would have been recorded from the same type of defective crystals, we would have observed a slower transformation kinetic on the lower side of the crystal as well.

C. Discussion

A polytypic transformation model involving the glide of partial dislocations has been suggested by Pirouz and Yang[12]. In the framework of this model, a pinned screw dislocation lying in the basal (111) plane dissociates into two partial dislocations with two different dislocation cores (a pure Si and pure C core), and hence different mobilities. The authors suggested that the Si(g) partial (where g indicates a dislocation from the glide set) is the most mobile and, under the action of shear stress, forms a faulted loop (i.e. the stacking sequence within the loop is changed) according to the Frank-Read mechanism, which progressively

faults the entire lattice plane upon the extension of this loop. Contrarily to a classical Frank-Read source, a second operation of the loop on the same plane is forbidden as this would violate the stacking rules by generating an AA-type stacking. Then, because of the overlap of the strain field of both partial dislocations, the dislocation undergoes a double cross-slip motion and thereby reaches the neighboring (111) plane, where a new faulted loop can be created. As outlined in Ref.[12], if this mechanism operates repeatedly and periodically, any polytypic sequence can be created starting from the 3C stacking. In the case of the 3C-6H transition, three successive faults are required with a periodicity of six planes, i.e. ABCABCABCABC... is transformed into ABCA|C|B|ABCA|C|B|... (the vertical bars indicate the SFs). When the initial screw dislocation (which is pinned in the primary glide plane) undergoes double cross-slip, it leaves a near-edge type 'residual' dislocation on the cross-slip plane. Such residual dislocations have been observed in 6H-SiC in the reverse 6H-3C transition[12] and have been considered as a strong indication of the validity of the model suggested by Pirouz and Yang. In its initial formulation this transformation mechanism requires the application of a shear stress in order to overcome the attractive force between the two partials which is itself due to the staking fault energy γ. However, since the publication of this model, there have been many studies demonstrating that the stacking fault energy in 3C-SiC is actually negative[34–36], which results in a repulsive force between the two partials, so that high temperatures may suffice to produce a faulted loop.

TEM experiments have been performed on a 3C-SiC crystals annealed at 1800°C for 2 hours (wafer 2), Fig. 6. Fig. 6(a,b) displays micrographs of cross-sectional 3C-SiC with [110] zone axis. Fig. 6 (a) shows typical high densities of SFs lying in 111 and elongated along <110> within the 3C-SiC crystal. Fig. 6 (b) zooms on a SF terminating within the crystal. This SF lies in (1 1 -1) and is bounded by a partial dislocation whose Burgers vector and line direction were determined to be 1/6[2 -1 1] and [2 9 11] (at 10° from [011]), respectively. The presence of SFs and the associated partial dislocations, which have been deduced from DXS experiments, are here clearly confirmed by TEM. An interesting feature is reported on another configuration in Fig. 6 (c) which shows dislocation segments lying out of (almost perpendicular to) the {111} primary glide plane. These segments (indicated by the white arrows) are very likely residual dislocations, which indicates that new SFs might have been generated in the crystal according to the mechanism of Pirouz and Yang[12]. The transformation kinetics obtained earlier can hence be interpreted in the light of this

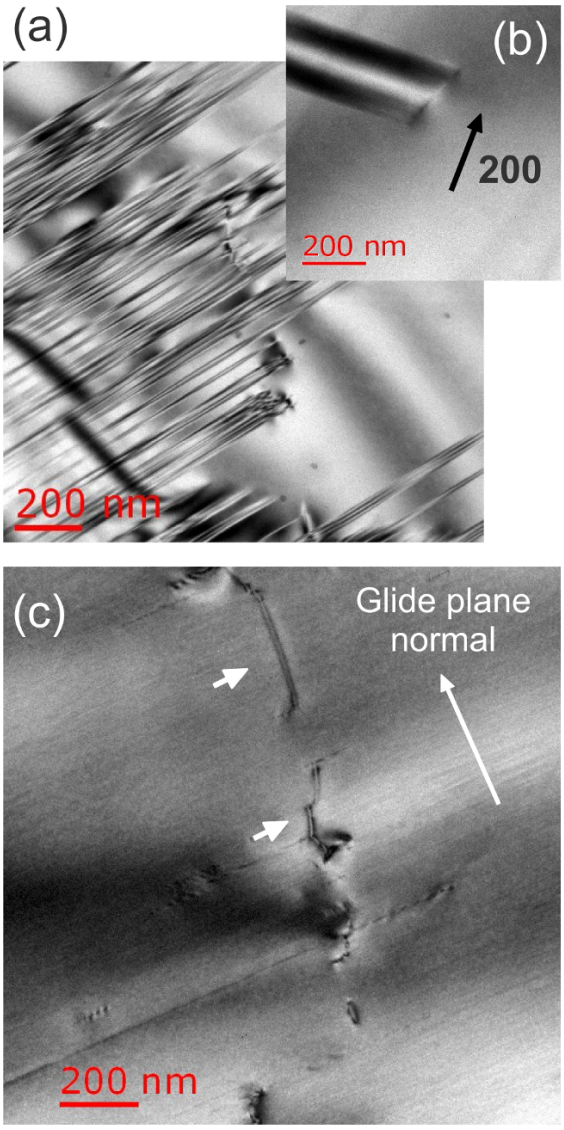

Figure 6. (a) Bright-field TEM image showing a region with a high density of large stacking faults lying in {111} in annealed 3C-SiC. (b) Detail of one stacking fault and the associated bounding partial dislocation. (c) Bright-field image of another area showing dislocation segments lying out of the {111} primary glide plane in a plane-view sample.

mechanism. Further investigation of these dislocation features are currently undertaken.

The parameter τ corresponds to the transformation level within bands of partially transformed material and is therefore solely dependent on the generation of new SFs according to the double cross-slip mechanism. The activation energy obtained for τ (1.5(1) eV on the upper side) therefore corresponds to the energy required to activate the double-cross slip

motion. Once new SFs are generated, the increase of the volume fraction of transformed material (x_t) requires the dislocation loops to glide over long distances (several hundreds of μm). The activation energy observed for x_t (0.5(4) eV on the upper side) therefore corresponds to the energy required to activate the glide of partial dislocations.

This process occurs in different places in the crystal and is continued until saturation is reached. It is however extremely unlikely that the transformation reaches completion. For τ to reach 100% a perfect periodic arrangement in the successive SFs is required which is by itself improbable. Moreover, when two different bands coalesce the stacking sequence within the first band must be perfectly continued in the second, which, taking into account the random distribution of the initial SF in the crystal, is also extremely unlikely. This explains why, in the best case, τ reaches a maximum of 90%. The situation is worse for x_t since in the most transformed crystal it only reaches 33%, i.e. even in the most transformed crystal 67% of the crystal volume corresponds to pure 3C. This slow kinetic can be explained by the fact that, in order to transform significant regions of the crystal, the dislocations have to glide over several hundred of μm, a path along which they might be pinned by structural defects. Moreover, two bands of transformed 3C, propagating in two different glide planes (say (111) and (-1-11)) cannot cross each other as they correspond to two distinct orientations of the upcoming 6H phase, so that the expansion of one band is stopped. Since this takes place randomly in the crystal volume, the complete conversion to a new polytype is obviously not possible.

We finally briefly discuss the activation energies obtained earlier. The activation energy of the double cross-slip mechanism (1.5(1) eV) is in remarkably good agreement with the value (1.54 eV) calculated by Käckell et al.[36] within an ab-initio density functional scheme. Concerning the activation energy for the glide of partial dislocations (0.5(4) eV), it can be noticed that it is lower than the values usually obtained in SiC, either in hexagonal polytypes as obtained from experiments[30,31], or in 3C-SiC using numerical simulations[32,33] (there is no experimental data for 3C-SiC). A value of 0.61 eV has been calculated by Savini et al.[37] for 90° C(g) partial dislocations using density functional theory, which is relatively close to our value. However, because of the significant scattering of the results obtained in these different studies, a formal identification of the dislocation type (in terms of the nature of the core, or core reconstruction) is not conceivable to date. Moreover, numerical studies predict the 90° C(g) partial to exhibit the lowest activation energy, and hence the highest mobility, whereas

the experimental evidence is that the 30°Si(g) are the most mobile. Further experiments are therefore required in order to identify the type of partials involved in the 3C-6H transition.

IV. CONCLUSION

The 3C-6H polytypic transition in 3C-SiC single crystals has been studied in details using diffuse X-ray scattering, supported by optical birefringence microscopy and transmission electron microscopy. It has been shown that high temperature annealing (in the 1700-2100°C range) sets off the 3C-6H transition which takes place by the nucleation of bands (parallel to the {111} planes) of partially transformed SiC. DXS allowed to determine both the transformation level within these partially transformed regions and the volume fraction corresponding to these regions. Prolonged thermal annealing induces the growth of these bands by the glide of partial dislocations, as well as the increase of the transformation level within the bands, by the multiplication of SFs through the double-cross slip process. It has further been shown that the generation of new SFs (with Ea = 1.5(1) eV) is a fast operating mechanism and is prominent at high temperatures (> 2000°C), whereas the glide of partial dislocation (with Ea = 0.5(4) eV) appears to be a much slower mechanism and dominates at lower temperatures (<2000°C).

ACKNOWLEDGMENTS

The authors would like to warmly thank the Region Limousin (France) for its financial support. LMGP thank the MINTEX-French ANR program (contract No. ANR-09-BLAN-0189-01) and the MANSiC-Marie Curie Research and Training Network (contract No. MRTN-CT-2006-035735) for their financial support.

REFERENCES

[1]H. Nagasawa, K. Yagi, T. Kawahara, and N. Hatta, Chem. Vap. Deposition **12**, 502 (2006).

[2]G. Alfieri, H. Nagasawa, and T. Kimoto, J. Appl. Phys. **106**, 073721 (2009).

[3]P. Scajev, V. Gudelis, K. Jarasiunas, and P. B. Klein, J. Appl. Phys. **108**, 023705 (2010).

[4]C. Wen, Y. M. Wang, W. Wan, F. H. Li, J. W. Liang, and J. Zou, J. Appl. Phys. **106**, 073522 (2009).

[5]M. A. Capano, B. C. Kim, A. R. Smith, E. P. Kvam, S. Tsoi, and A. K. Ramdas, J. Appl. Phys. **100**, 083514 (2006).

[6]Y. Ishida, T. Takahashi, H. Okumura, and S. Yoshida, J. Appl. Phys. **94**, 4676 (2003).

[7]H. Nagasawa, M. Abe, K. Yagi, T. Kawahara, and N. Hatta, Phys. Status Solidi B **245**, 1272 (2008).

[8]J. W. Sun, G. Zoulis, J. C. Lorenzzi, N. Jegenyes, H. Peyre, S. Juillaguet, V. Souliere, F. Milesi, G. Ferro, and J. Camassel, J. Appl. Phys. **108**, 013503 (2010).

[9]M. Eickhoff, H. Möller, J. Stoemenos, S. Zappe, G. Kroetz, and M. Stutzmann, J. Appl. Phys. **95**, 7908 (2004).

[10]A. A. Porporati, K. Hosokawa, W. Zhu, and G. Pezzotti, J. Appl. Phys. **100**, 093508 (2006).

[11]N. W. Jepps and T. F. Page, Prog. Cryst. Growth Charact. Mater. **7**, 259 (1983).

[12]P. Pirouz and J. W. Yang, Ultramicroscopy **51**, 189 (1993).

[13]W. S. Yoo and H. Matsunami, J. Appl. Phys. **70**, 7124 (1991).

[14]R. Püsche, M. Hundhausen, L. Ley, K. Semmelroth, F. Schmid, G. Pensl, and H. Nagasawa, J. Appl. Phys. **96**, 5569 (2004).

[15]V. K. Kabra, D. Pandey, and S. Lele, J. Mater. Sci. **21**, 1654 (1986).

[16]A. Boulle, J. Aube, I. G. Galben-Sandulache, and D. Chaussende, Appl. Phys. Lett. **94**, 201904 (2009).

[17]H. Nagasawa, K. Yagi, and T. Kawahara, J. Cryst. Growth **237**, 1244 (2002).

[18]E. Polychroniadis, M. Syväjärvi, R. Yakimova, and J. Stoemenos, J. Cryst. Growth **263**, 68 (2004).

[19]A. Boulle, D. Chaussende, F. Conchon, G. Ferro, and O. Masson, J. Cryst. Growth **310**, 982 (2008).

[20]A. Boulle, D. Chaussende, L. Latu-Romain, F. Conchon, O. Masson, and R. Guinebretière, Appl. Phys. Lett. **89**, 091902 (2006).

[21]A. Boulle, O. Masson, R. Guinebretière, and A. Dauger, Appl. Surf. Sci. **180**, 322 (2001).

[22]A. Boulle, O. Masson, R. Guinebretière, A. Lecomte, and A. Dauger, J. Appl. Cryst. **35**, 606 (2002).

[23]A. Boulle, D. Dompoint, I. Galben-Sandulache, and D. Chaussende, J. Appl. Cryst. **43**, 867 (2010).

[24]B. E. Warren, X-Ray Diffraction, New-York: Addison-Wesley, (1969).

[25]B. I. Nikolin and A. Yu. Babkevich, Acta Cryst.A **45**, 797 (1989).

[26]D. Chaussende, F. Mercier, R. Madar, and M. Pons, Mater. Sci. Forum **600**, 71 (2009).

[27]H. Holloway, J. Appl. Phys. **40**, 4313 (1969).

[28]A. Boulle, F. Conchon, and R. Guinebretière, Acta Cryst.A **62**, 11 (2006).

[29]A. Boulle, R. Guinebretière, and A. Dauger, J. Phys. D: Appl. Phys. **38**, 3907 (2005).

[30]A. V. Samant, M. H. Hong, and P. Pirouz, Phys. Status Solidi B **222**, 75 (2000).

[31]H. Idrissi, B. Pichaud, G. Regula, and M. Lancin, J. Appl. Phys. **101**, 113533 (2007).

[32]P. K. Sitch, R. Jones, S. Berg, and M. I. Heggie, Phys. Rev. B **52**, 4951 (1995).

[33]A. T. Blumenau, C. J. Fall, R. Jones, S. Öberg, T. Frauenheim, and P. R. Briddon, Phys. Rev. B **68**, 174108 (2003).

[34]H. P. Iwata, U. Lindefelt, S. Öberg, and P. R. Briddon, Phys. Rev. B **68**, 113202 (2003).

[35]U. Lindefelt, H. Iwata, S. Öberg, and P. R. Briddon, Phys. Rev. B **67**, 155204 (2003).

[36]P. Käckell, J. Furthmüller, and F. Bechstedt, Phys. Rev. B **60**, 13261 (1999).

[37]G. Savini, M. I. Heggie, and S. Öberg, Faraday Discuss. **134**, 353 (2007).